







This article may be downloaded for personal use only. Any other use requires prior permission of the author and AIP Publishing. This article appeared in Tiehan Long, Peixu Guo, Rui Zhao, Chihyung Wen, Feng Ji; Energy growth of vortical, acoustic, and entropic components of the second-mode instability in the hypersonic boundary layer. Physics of Fluids 1 May 2023; 35 (5): 054104 and may be found at <https://dx.doi.org/10.1063/5.0141414>.

RESEARCH ARTICLE | MAY 01 2023

Energy growth of vortical, acoustic, and entropic components of the second-mode instability in the hypersonic boundary layer

Special Collection: [Hypersonic Flow](#)

Long Tiehan (龙铁汉) ; Guo Peixu (郭培旭) ; Zhao Rui (赵瑞)  ; Wen Chihyung (温志湧) ; Ji Feng (纪锋) 

 Check for updates

Physics of Fluids 35, 054104 (2023)

<https://doi.org/10.1063/5.0141414>



27 August 2024 06:12:57



Physics of Fluids

Special Topic:

Kitchen Flows 2024

Guest Editors: Gerald G. Fuller, Maciej Lisicki, Arnold J.T.M. Mathijssen, Endre Joachim Mossige, Rossana Pesquino, Vivek Nagendra Prakash, Laurence Ramos

[Submit Today!](#)

Energy growth of vortical, acoustic, and entropic components of the second-mode instability in the hypersonic boundary layer

Cite as: Phys. Fluids **35**, 054104 (2023); doi: [10.1063/5.0141414](https://doi.org/10.1063/5.0141414)

Submitted: 5 January 2023 · Accepted: 11 April 2023 ·

Published Online: 1 May 2023



View Online



Export Citation



CrossMark

Tiehan Long (龙铁汉),¹  Peixu Guo (郭培旭),²  Rui Zhao (赵瑞),^{3,a)}  Chihyung Wen (温志湧),² 
and Feng Ji (纪锋)¹ 

AFFILIATIONS

¹China Academy of Aerospace Aerodynamics, Beijing, China

²Department of Aeronautical and Aviation Engineering, The Hong Kong Polytechnic University, Hung Hom, Kowloon, Hong Kong, China

³School of Aerospace Engineering, Beijing Institute of Technology, Beijing 100081, China

Note: This paper is part of the special topic, Hypersonic Flow.

^{a)} Author to whom correspondence should be addressed: zr@bit.edu.cn

ABSTRACT

The acoustic, vortical, and entropic (thermal) components of the second-mode instability, regarded as an asymptotic behavior of the free-stream counterparts, were found to interact with each other in a well-defined way. However, the mechanisms of the energy growth of each component and the resulting second mode instability remain to be clarified. The present paper provides a quantitative energy analysis of the key sources responsible for the modal growth in the momentum potential theory framework. The acoustic, vortical, and entropic components are governed by energy source effects and interexchange effects, characterized by explicit transport terms and relationships between the growth rate and the energy source. The thermal-acoustic source, induced by the interaction between the fluctuation pressure and the fluctuation entropy, is revealed to be the most pronounced cause of the second-mode instability in the hypersonic boundary layer. The thermal-acoustic source is further decomposed into the dissipative (viscous) part and the non-dissipative (inviscid) part. The dissipative thermal-acoustic source is dominant near the wall surface and destabilizes the second mode. The non-dissipative thermal-acoustic source destabilizes the second mode significantly at the critical layer, while the dissipative thermal-acoustic source stabilizes the second mode in this region.

Published under an exclusive license by AIP Publishing. <https://doi.org/10.1063/5.0141414>

I. INTRODUCTION

It is well known that the transition from laminar to turbulent in the hypersonic boundary layer is crucial to the design of hypersonic vehicles.¹ Premature transition increases heating to the vehicle surface significantly, which is highly challenging to the thermal protection system (TPS) design. The laminar–turbulent transition in the hypersonic boundary layer in low-disturbance environments is primarily caused by the modal growth of instability modes.² Numerous experimental investigations,^{3–7} linear stability theory (LST) studies,^{8–12} and numerical simulations^{13–17} have been conducted to study the modal growth of hypersonic boundary layer instability modes. Mack⁸ first identified that multiple instability modes co-exist in the hypersonic boundary layer at a high Mach number, typically like Mach number $M > 4$. In addition, wall cooling can make the second mode dominant at a lower Mach number. In the supersonic boundary layer, the first mode can be

regarded as the counterpart of the Tollmien–Schlichting mode. The second and higher modes are high-frequency sound waves trapped in the waveguide between the solid wall and the sonic line.¹

The theoretical study by LST shows the existence of unstable modes in the hypersonic boundary layer by mathematically giving the growth rate of these modes. However, it is still a mystery how these unstable modes are amplified downstream from a physical perspective. There have been attempts to provide a physical interpretation of the growth of small disturbances in the flow field based on energy approaches. Reynolds¹⁸ proposed a two-dimensional (2D) kinetic energy equation for incompressible parallel shear flows. The total disturbance kinetic energy growth rate is related to a production term due to the Reynolds stress and a dissipation term due to the viscous effect. The small 2D disturbance in the incompressible boundary layer grows if and only if the production term outweighs the dissipation

term. Kuehl¹⁹ derived a Lagrangian acoustic energy equation by ignoring the viscous effect for the compressible boundary layer. With the Lagrangian acoustic energy equation, Kuehl showed that the second mode is related to a forced, resonating, thermo-acoustic standing wave trapped in a thermo-acoustic impedance well formed by the sonic line and the solid wall. The thermo-acoustic Reynolds stress draws energy from the mean flow, which is the energy source for the amplification of the second mode. Tian and Wen²⁰ performed the stability analysis for the second mode in a Mach 6.0 boundary layer based on the fluctuating internal energy. The second mode has the largest growth rate when the wall-normal transport of energy is in phase to the change in fluctuating internal energy in the vicinity of the critical layer, similar to the mechanism of the Rijke tube that “depends upon the phase of the vibration at which the transfer of heat takes place.”²¹ With the energy approach, the results of Kuehl¹⁹ and Tian²⁰ provide some insight into the physical mechanism of the second mode from different perspectives. However, their results do not explicitly present the relation between the growth rate of the second mode and energy sources. This point is one of the motivations and contributions of the present paper.

The other motivation is that the aforementioned energy analyses ignored the earlier evolution of the second mode instability wave through the receptivity process. It is well known that infinitesimal free-stream disturbances can be decomposed into different modes, including the vortical, acoustic, and entropic components, and each of them is governed by an individual equation.²² However, when the three types of free-stream disturbances enter the boundary layer, they couple with each other and the base flow in quite a complicated manner. Therefore, although the evolution of the second mode is closely linked with the slow acoustic waves and others,¹⁶ the energy analysis considering the decomposed components is difficult to perform. Recently, Unnikrishnan and Gaitonde²³ utilized the momentum potential theory (MPT) to decompose the second mode into the vortical, acoustic, and entropic components and found that they interact with each other and the base flow in a well-described process. The highlight is that the MPT technique provides a straightforward way to reveal the coupling of the three components without the leading-edge receptivity analysis. In detail, the momentum potential theory (MPT) proposed by Doak²⁴ obtained an energy budget equation for disturbances in a time-stationary mean flow field. The fluctuation momentum density is decomposed into vortical, acoustic, and thermal components. The transport of the total energy flux is governed by the superimposition of the source terms due to each MPT component and an additional source term. The vortical component displays a series of rope-shaped recirculation-cell patterns in the boundary layer, while both acoustic and thermal components display “trapped” structures. Furthermore, Unnikrishnan and Gaitonde examined source terms in the boundary layer with different wall temperatures based on the MPT’s energy budget equation and claimed that the thermal source is the primary source for the growth of the second mode. The finding of Unnikrishnan and Gaitonde is inspiring. However, their conclusion that the modal growth of the second mode is caused by the thermal source is mainly based on numerical observations of the term magnitude itself. The work lacks a direct link between the growth rate and source terms in Doak’s energy budget equation, yielding a debatable question. Long *et al.*²⁵ applied MPT to study the sound radiation mechanism of the supersonic mode in a Mach 6.0 boundary layer over the highly cooled wall. Doak’s energy budget equation is developed into three independent energy budget

equations for each MPT component. The effect of different source terms on each energy flux was clarified, and energy exchange terms between different MPT components were revealed.

In the present study, having considered the decomposition into vortical, acoustic, and entropic components, direct evidence is shown on the dominant energy source of the second mode instability by establishing explicit relationships between the growth rate and the energy source terms. The LST results of the Mach 6.0 boundary layer with different wall temperatures and different Reynolds numbers are analyzed with MPT. The modal growth of the second mode is studied by developing an integrated form of the MPT energy budget equation to establish a direct link between the growth rate and MPT sources, which enables a quantitative analysis of the contribution of MPT sources to the modal growth of the second mode. The roles of different source terms in the amplification of the second mode are, thus, identified intuitively and systematically for the first time.

II. MOMENTUM POTENTIAL THEORY

For clarity of the context, Doak’s momentum potential theory is briefly summarized as follows: The momentum density \mathbf{m} ($\equiv \rho\mathbf{u}$, ρ is density, \mathbf{u} is the velocity vector) is selected as the primary dependent vector field to be decomposed. According to the Helmholtz theorem, the vector field \mathbf{m} can be split into its solenoidal vortical component \mathbf{m}_B and an irrotational component. The latter can be expressed as a gradient of a scalar potential $-\psi$

$$\mathbf{m} \equiv \rho\mathbf{u} = \mathbf{m}_B - \nabla\psi, \quad \nabla \cdot \mathbf{m}_B = 0. \quad (1)$$

For a time-stationary flow field, any instantaneous flow quantity f consists of a mean part (denoted by \bar{f}) and a fluctuation part (denoted by f') as follows:

$$\bar{\mathbf{m}} = \bar{\mathbf{m}}_B - \nabla\bar{\psi}, \quad \mathbf{m}' = \mathbf{m}_B - \nabla\psi'. \quad (2)$$

The mean continuity equation and the fluctuation continuity equation can be expressed as follows:

$$\nabla \cdot \bar{\mathbf{m}} = 0, \quad \frac{\partial \rho'}{\partial t} + \nabla \cdot \mathbf{m}' = 0. \quad (3)$$

The mean momentum density $\bar{\mathbf{m}}$ is divergence-free. By substituting the corresponding Eq. (2) into Eq. (3), the mean scalar potential $\bar{\psi}$ can be assumed to be zero, and a Poisson equation is obtained for the scalar potential of fluctuation as follows:

$$\frac{\partial \rho'}{\partial t} = \nabla^2 \psi'. \quad (4)$$

For a single-chemical-component continuum in the thermal equilibrium state, the density ρ can be defined as a function of the thermodynamic pressure p and entropy S as follows:

$$\rho = \rho(p, S). \quad (5)$$

Consequently,

$$\frac{\partial \rho'}{\partial t} = \frac{\partial \rho}{\partial p} \frac{\partial p'}{\partial t} + \frac{\partial \rho}{\partial S} \frac{\partial S'}{\partial t}, \quad \frac{\partial \rho}{\partial p} = \frac{1}{\gamma RT}, \quad \frac{\partial \rho}{\partial S} = -\frac{(\gamma - 1)\rho}{\gamma R}. \quad (6)$$

Hence, the scalar potential ψ' can be assumed to be a linear superposition of an acoustic potential ψ'_A and a thermal potential ψ'_T as follows:

$$\psi' = \psi'_A + \psi'_T, \quad \frac{1}{\gamma RT} \frac{\partial p'}{\partial t} = \nabla^2 \psi'_A, \quad -\frac{(\gamma - 1)\rho}{\gamma R} \frac{\partial S'}{\partial t} = \nabla^2 \psi'_T. \quad (7)$$

The fluctuation momentum density \mathbf{m}' is, therefore, expressed as a superposition of the vortical component \mathbf{m}'_B , acoustic component \mathbf{m}'_A , and thermal component \mathbf{m}'_T ,

$$\mathbf{m}' = \mathbf{m}'_B + \mathbf{m}'_A + \mathbf{m}'_T, \quad \mathbf{m}'_A = -\nabla \psi'_A, \quad \mathbf{m}'_T = -\nabla \psi'_T. \quad (8)$$

In this study, the Poisson equations for ψ' and ψ'_A are solved. Subsequently, ψ'_T and \mathbf{m}'_B are obtained using $\psi'_T = \psi' - \psi'_A$ and $\mathbf{m}'_B = \mathbf{m}' - \mathbf{m}'_A - \mathbf{m}'_T$, respectively. The Dirichlet boundary conditions for the Poisson equations are formulated by integration along the boundaries, as in Unnikrishnan and Gaitonde²³ and Daviller *et al.*²⁶

Another critical aspect of the Doak's MPT approach is the energy budget equation, which can be written as follows:

$$\nabla \cdot \overline{H'\mathbf{m}'} = -\overline{\mathbf{m}' \cdot \boldsymbol{\zeta}'} + \frac{\overline{p' \partial S'}}{R \partial t}, \quad (9)$$

where $\overline{H'\mathbf{m}'}$ is the mean energy flux.

The total fluctuation enthalpy H' and the acceleration vector $\boldsymbol{\zeta}'$ are defined as follows:

$$H' = \left(C_p T + \frac{\mathbf{u} \cdot \mathbf{u}}{2} \right)', \quad \boldsymbol{\zeta}' = (\boldsymbol{\Omega} \times \mathbf{u})' - \left(T \nabla S + \frac{1}{\rho} \nabla \cdot \boldsymbol{\tau} \right)', \quad (10)$$

where $\boldsymbol{\Omega}$ and $\boldsymbol{\tau}$ denote the vorticity vector and the viscous stress tensor, respectively. C_p is the specific heat at constant pressure, and T is temperature.

Because the fluctuation momentum density \mathbf{m}' is a superposition of the vortical, acoustic, and thermal components, the term $\mathbf{m}' \cdot \boldsymbol{\zeta}'$ can be split into multiple source terms due to different components. Substituting Eq. (8) into Eq. (9) yields

$$\nabla \cdot \overline{H'\mathbf{m}'} = -\left(\overline{\mathbf{m}'_B \cdot \boldsymbol{\zeta}'} + \overline{\mathbf{m}'_A \cdot \boldsymbol{\zeta}'} + \overline{\mathbf{m}'_T \cdot \boldsymbol{\zeta}'} \right) + \frac{\overline{p' \partial S'}}{R \partial t}. \quad (11)$$

The left-hand-side term in Eq. (11) is the divergence of the mean energy flux. The first three terms on the right-hand side indicate energy sources due to the interaction of the vector $\boldsymbol{\zeta}'$ with different MPT components. In addition to the source terms due to the MPT components, the source term, $\frac{\overline{p' \partial S'}}{R \partial t}$, is the interaction between fluctuation pressure and entropy. It is noted that fluctuation pressure and entropy are related to the acoustic and thermal components in Eq. (7), respectively. Thus, the source, $\frac{\overline{p' \partial S'}}{R \partial t}$, represents the thermo-acoustic coupling effect in the disturbances flow field. For convenience of discussion, the vortical source $-\overline{\mathbf{m}'_B \cdot \boldsymbol{\zeta}'}$, acoustic source $-\overline{\mathbf{m}'_A \cdot \boldsymbol{\zeta}'}$, and thermal source $-\overline{\mathbf{m}'_T \cdot \boldsymbol{\zeta}'}$ are designated as P_B , P_A , and P_T , respectively. The source due to the thermo-acoustic coupling effect is designated as P_{ta} .

III. GROWTH RATE IN MPT

The growth rate analysis was performed on the second mode obtained from 2D spatial LST because the most unstable second mode

is two-dimensional, while the most unstable first mode is oblique (the first mode with a wave angle close to 60° has the largest amplification rate at $M = 4.5$ with insulated wall⁸). Considering instability modes in a two-dimensional (2D) spatial LST, Eq. (11) can be rewritten as follows (see Appendixes A and B for details):

$$2\sigma \overline{(\rho u)'H'} + \frac{\partial \overline{(\rho v)'H'}}{\partial y} = P_B + P_A + P_T + P_{ta}. \quad (12)$$

Here, u is the streamwise velocity, v is the surface normal velocity, and $\sigma = -\alpha_i$ is the growth rate in the 2D spatial LST. α_i is the imaginary part of the complex wavenumber α in the 2D spatial LST. There are two terms: $2\sigma \overline{(\rho u)'H'}$ and $\frac{\partial \overline{(\rho v)'H'}}{\partial y}$ on the left-hand side of Eq. (12). Consequently, it is difficult to clarify the effect of different source terms on the growth rate σ . To eliminate the y derivative term, Eq. (12) is integrated from $y = 0$ to $y \rightarrow +\infty$ with the following boundary condition:

$$\begin{cases} y = 0 : (\rho v)' = 0 \\ y \rightarrow +\infty : (\rho v)' = 0 \end{cases} \Rightarrow \int_0^{+\infty} \frac{\partial \overline{(\rho v)'H'}}{\partial y} dy = \overline{(\rho v)'H'}|_{y \rightarrow \infty} - \overline{(\rho v)'H'}|_{y=0} = 0. \quad (13)$$

Finally, we have

$$2\sigma \int_0^{+\infty} \overline{(\rho u)'H'} dy = \int_0^{+\infty} P_B dy + \int_0^{+\infty} P_A dy + \int_0^{+\infty} P_T dy + \int_0^{+\infty} P_{ta} dy. \quad (14)$$

Furthermore, Eq. (14) is rewritten as follows:

$$\begin{aligned} \sigma &= \frac{\int_0^{+\infty} P_B dy + \int_0^{+\infty} P_A dy + \int_0^{+\infty} P_T dy + \int_0^{+\infty} P_{ta} dy}{2Q_x} \\ &= \sigma_B + \sigma_A + \sigma_T + \sigma_{ta}. \end{aligned} \quad (15)$$

Here, $\int_0^{+\infty} \overline{(\rho u)'H'} dy = Q_x$. The contribution of each source term to the growth rate σ is defined as follows:

$$\begin{aligned} \sigma_B &= \frac{\int_0^{+\infty} P_B dy}{2Q_x}, \quad \sigma_A = \frac{\int_0^{+\infty} P_A dy}{2Q_x}, \quad \sigma_T = \frac{\int_0^{+\infty} P_T dy}{2Q_x}, \\ \sigma_{ta} &= \frac{\int_0^{+\infty} P_{ta} dy}{2Q_x}. \end{aligned} \quad (16)$$

IV. LINEAR STABILITY ANALYSIS

In the 2-D spatial LST with the parallel flow assumption, the small disturbance is expressed by the traveling-wave form of $\phi'(x, y, t) = \hat{\phi}(y)e^{i(\omega t - \alpha x)}$. The circular frequency ω is real, the wavenumber α is complex, and $\hat{\phi}(y)$ is the complex eigenfunction.

The linearized Navier–Stokes equations for small disturbances are written in the matrix form¹¹ as follows:

$$\frac{\partial}{\partial y} \left(L_0 \frac{\partial \hat{\phi}}{\partial y} \right) + L_1 \frac{\partial \hat{\phi}}{\partial y} = H_1 \hat{\phi} + i\alpha H_2 \hat{\phi}. \quad (17)$$

Here, vector $\hat{\phi} = (\hat{u}, \frac{\partial \hat{u}}{\partial y}, \hat{v}, \hat{p}, \hat{T}, \frac{\partial \hat{T}}{\partial y}, i\alpha \hat{u}, i\alpha \hat{v}, i\alpha \hat{T})^T$. L_0, L_1, H_1 , and H_2 are 9×9 matrices.

The boundary condition for Eq. (17) is as follows:

$$\begin{cases} y = 0 : \hat{u} = \hat{v} = \hat{T} = 0 \\ y \rightarrow \infty : |\hat{u}| = |\hat{v}| = |\hat{T}| = 0. \end{cases} \quad (18)$$

Finally, Eq. (17) is discretized along with boundary conditions (18). A matrix eigenvalue problem is formulated as follows:

$$A\hat{\phi} = i\alpha B\hat{\phi}. \quad (19)$$

In the present 2-D spatial LST, dimensional flow parameters are normalized by the steady-state free-stream conditions. Specifically, velocities are normalized by the free stream velocity u_∞^* , temperature by the free stream temperature T_∞^* , density by the free stream density ρ_∞^* , and pressure by $\rho_\infty^* u_\infty^{*2}$. The characteristic length used to normalize length scales is the local boundary layer thickness $L_{ref} = \sqrt{\frac{x^*}{Re_u}}$, where x^* is the distance from the leading edge of the flat plate and Re_u is the unit Reynolds number. The superscript “*” represents dimensional variables. In the following texts, the Reynolds number Re is based on the reference scale L_{ref} . The gas is assumed to be calorically and thermally perfect with $Pr = 0.72$ and $\gamma = 1.4$. The viscosity μ^* is approximated by Sutherland’s law,

$$\frac{\mu^*}{\mu_{ref}^*} = \frac{T_{ref} + a}{T^* + a} \left(\frac{T^*}{T_{ref}} \right)^{1.5}, \quad (20)$$

where $a = 110.4\text{ K}$ is a constant, the reference temperature is $T_{ref} = 273.15\text{ K}$, and the reference viscosity is $\mu_{ref} = 1.716 \times 10^{-5}\text{ Pa s}$.

Two-dimensional spatial LST analyses are performed to calculate the eigenmode for the canonical $M = 6.0$ flat plate boundary layer case, and then, MPT components and source terms are extracted from the LST mode and analyzed in detail. In the present paper, only mode S is considered since in most cases it evolves into the unstable second mode.²⁷ First, the $M = 6.0$ flat plate boundary layer over the adiabatic wall with $Re = 1000, 5000$, and 9000 is studied to reveal the viscous effect on the modal growth of the second mode. The free stream temperature $T_\infty^* = 300\text{ K}$. In this case, the recovery temperature is

$T_r \approx 7.02 T_\infty^*$. Afterward, LST analyses of three cases with wall temperatures $T_w = 0.7 T_r, 1.0 T_r$ (adiabatic wall), and $1.3 T_r$ at $Re = 5000$ are performed to take the wall temperature effect into consideration. Self-similar solutions of the steady state of the Mach 6.0 flat plate boundary layer with $T_w = 0.7 T_r, 1.0 T_r$, and $1.3 T_r$ are plotted in Fig. 1. Here, Y is the non-dimensional wall normal coordinate by the local boundary layer thickness L_{ref} . It is evident that wall temperature significantly affects the boundary layer thickness. The boundary layer is thicker with higher wall temperature.

Figure 2 shows 2D spatial results of the Mach 6.0 flat plate boundary layer over the adiabatic wall with $Re = 1000, 5000$, and 9000 . Nondimensional phase speed $C_{ph} = \frac{\omega}{\alpha_r}$ of two discrete modes is plotted in Fig. 2(a). Three horizontal dashed dotted lines indicate the phase speed of fast acoustic waves (upper, $C_{ph} = 1 + \frac{1}{M}$), entropy/vorticity waves (middle, $C_{ph} = 1$), and slow acoustic waves (lower, $C_{ph} = 1 - \frac{1}{M}$) in the free stream. Two discrete modes exist in the 2D spatial LST results. The fast mode (mode F) has the same phase speed as fast acoustic waves at the leading edge (non-dimensional circular frequency $\omega = \frac{\omega^*}{u_\infty^*} \sqrt{\frac{x^* \mu_\infty^*}{\rho_\infty^* u_\infty^*}} = 0$ in Fig. 2), while the slow mode (mode S) has the same phase speed as slow acoustic waves here.²⁷ The mode F synchronizes with the Mode S at $\omega \approx 0.156, 0.157$, and 0.158 with $Re = 1000, 5000$, and 9000 , respectively. The non-dimensional growth rate σ of the modes F and S is plotted Fig. 2(b). The mode S is unstable and has the largest growth rate at $\omega \approx 0.159, 0.166$, and 0.166 with $Re = 1000, 5000$, and 9000 , respectively. The mode S evolves into the second mode in the vicinity of the synchronization point,²⁷ where the mode S has the same phase speed as the Mode F, in the considered case. Downstream of the synchronization point, the mode S is more unstable with a larger Re .

Figure 3 shows 2D spatial results of the Mach 6.0 flat plate boundary layer with $T_w = 0.7 T_r, 1.0 T_r$, and $1.3 T_r$ at $Re = 5000$. The mode F synchronizes with the mode S at $\omega \approx 0.157$ with different T_w . The cold wall destabilizes the second mode (the mode S around the synchronization point) significantly, while the hot wall stabilizes the second mode. The most unstable second mode locates at $\omega \approx 0.171, 0.166$, and 0.162 , respectively.

V. GROWTH RATE ANALYSIS OF THE MODE S

Because the second mode in present cases is related to the unstable mode S where the synchronization occurs,¹ the mode S obtained

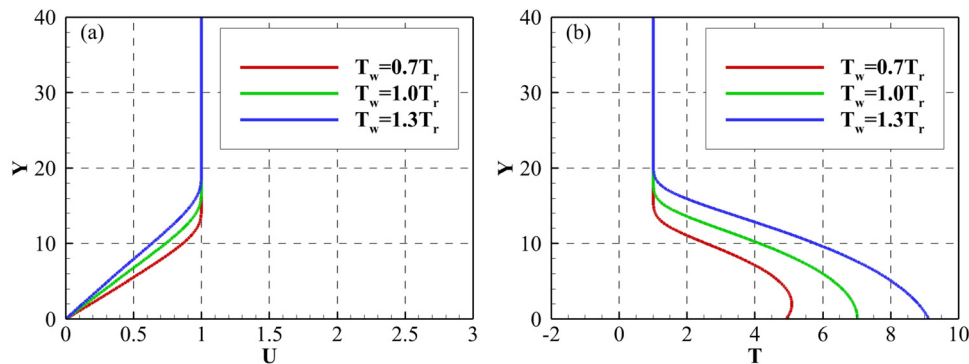


FIG. 1. Distributions of (a) streamwise velocity and (b) temperature in the Mach 6.0 flat plate boundary layer with different wall temperatures.

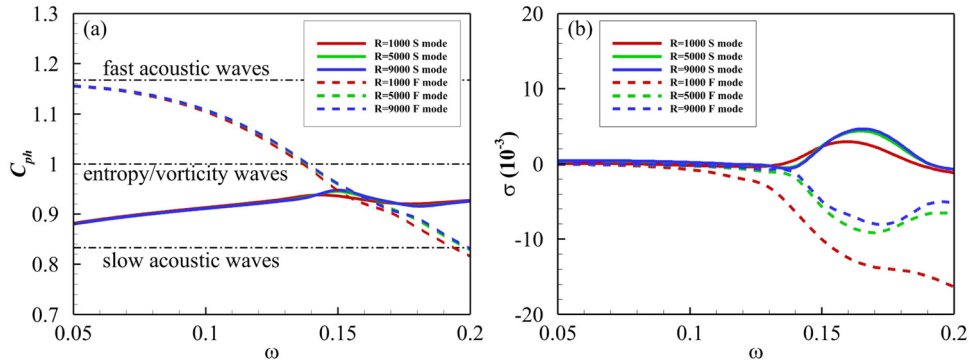


FIG. 2. (a) Phase speed $C_{ph} = \frac{\omega}{\alpha_r}$ and (b) growth rate $\sigma = -\alpha_i$ of the mode S and the mode F in the Mach 6.0 boundary layer over the adiabatic wall with different Re. ω is the non-dimensional circular frequency.

from LST is analyzed by MPT in Secs. V and VI. For convenience of discussion, the notation $q_x = (\rho u)'H'$ is adopted. It is noted that $Q_x = \int_0^\infty q_x dy$ appears in Eqs. (15) and (16) as denominators, which makes an essential difference in the contribution of MPT sources to the amplification of the second mode. Figure 4 shows $\frac{q_x}{|Q_x|}$ of the mode S at $\omega = 0.1$ (lower frequency than the second mode), 0.15 (in the region of the second mode), and 0.2 (higher frequency than the second mode) with different wall temperature and R . In all cases, the magnitude of $\frac{q_x}{|Q_x|}$ is relatively small in most regions of the boundary layer near the wall and becomes negative with a large magnitude near the boundary layer edge. Consequently, Q_x is negative for the mode S. Based on Eq. (15), the results indicate that negative MPT sources in conjunction with a negative Q_x eventually destabilize the mode S.

Figure 5 shows the distribution of MPT sources of the mode S normalized by $2Q_x$. There exists a negative correlation between $\frac{P_B}{2Q_x}$ and $\frac{P_T}{2Q_x}$. This observation is consistent with the results of Unnikrishnan and Gaitonde,²³ and they attribute this phenomenon to the vortical-entropy coupling effect. MPT sources are significant near the wall and around the critical layer ($u = C_{ph}$). Here, the critical layer is the location where singularity occurs in the inviscid stability

equations and the solution is still large in the complete viscous theory. Another important observation is that $\frac{P_{ta}}{2Q_x}$ is positive everywhere in all cases, which indicates that the thermal-acoustic source P_{ta} always destabilizes the mode S.

The contribution of MPT sources to the growth rate σ of the mode S over the adiabatic wall with different Re is plotted in Fig. 6. The vertical dashed-dotted line indicates the synchronization point (SP) of the modes F and S. In all cases with different Re, σ_{ta} and σ_B are positive, while σ_A and σ_T are negative. The thermal-acoustic source P_{ta} and the vortical source P_B destabilize the mode S while the acoustic source P_A and the thermal source P_T stabilize the mode S. For all three cases with different Re, similar tendencies are shown which may indicate a universal law in this state. More importantly, the term σ_{ta} , yielded by the thermal-acoustic source, is the most pronounced positive contribution among all in the vicinity of the SP. It has been shown by Fedorov¹ that the synchronization between the fast and slow modes signifies the unstable second mode. Consequently, Fig. 6 provides direct evidence that the thermal-acoustic source is highly important in the evolution of the second mode instability. The contribution of MPT sources to the growth rate σ of the mode S at Re = 5000 with different wall temperatures are also plotted in Fig. 7.

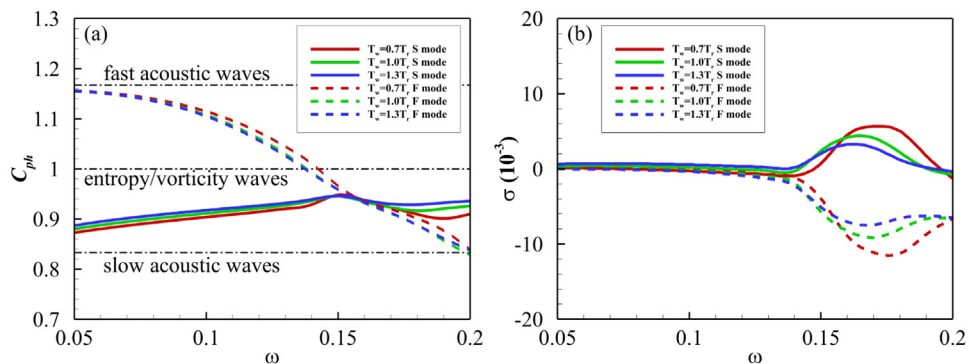


FIG. 3. (a) Phase speed $C_{ph} = \frac{\omega}{\alpha_r}$ and (b) growth rate $\sigma = -\alpha_i$ of the mode S and the mode F in the Mach 6.0 boundary layer with wall temperature $T_w = 0.7 T_r$, $1.0 T_r$, and $1.3 T_r$ at Re = 5000.

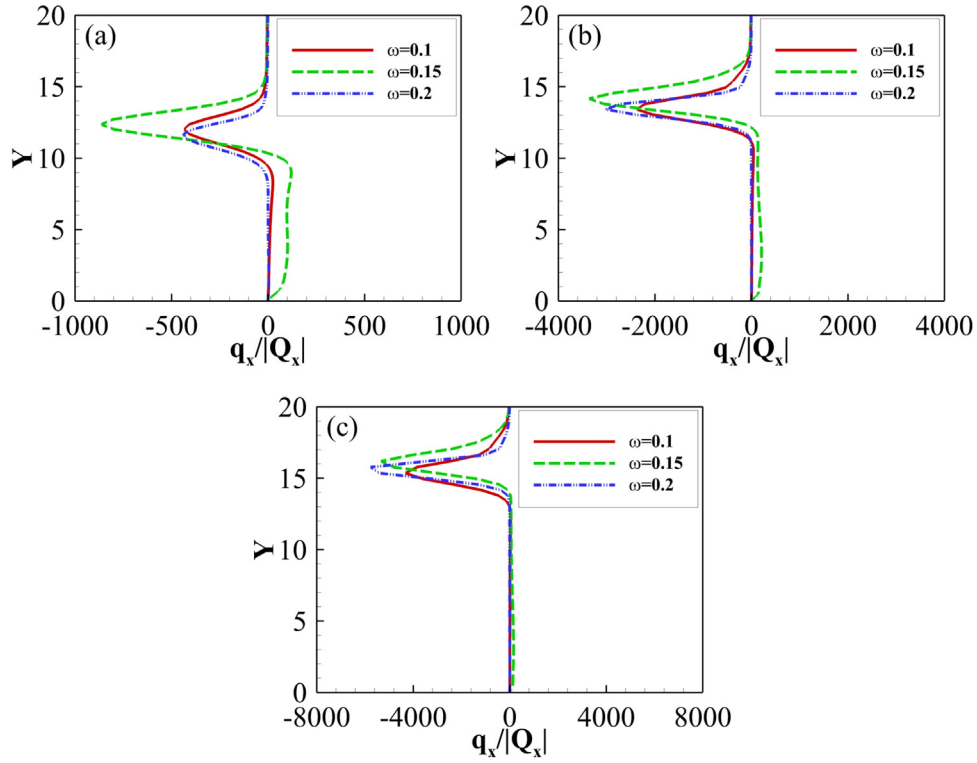


FIG. 4. $\frac{\text{Re}(\sigma_s)}{|Q_x|}$ of the mode S at $\omega = 0.1, 0.15,$ and 0.2 with (a) $\text{Re} = 1000$ and $T_w = 0.7 T_r$; (b) $\text{Re} = 5000$ and $T_w = 1.0 T_r$; (c) $\text{Re} = 9000$ and $T_w = 1.3 T_r$.

The results are similar to those in Fig. 6. A notable difference is that the magnitude of $\sigma_A, \sigma_B, \sigma_T,$ and σ_{ta} is larger with lower wall temperature. Meanwhile, the role of the peak σ_{ta} is not affected by the wall cooling effect, which makes the conclusion more general and convincing.

The negative correlation between σ_B and σ_T is attributed to the negative correlation between vortical source P_B and thermal source P_T due to the vortical-entropy coupling effect (see Fig. 5). The acoustic source P_A is not correlated with the thermal-acoustic source P_{ta} in Fig. 5, while their contribution to the growth rate σ_A and σ_{ta} is negatively correlated in Figs. 6 and 7. In author’s previous MPT work on the supersonic mode,²⁵ the independent energy budget equation for each MPT component is developed in the following form:

$$\begin{cases} \nabla \cdot \overline{H'm'_B} = P_B + Ex_{AB} + Ex_{TB} \\ \nabla \cdot \overline{H'm'_A} = P_A + Ex_{BA} + Ex_{TA} + \frac{P_{ta}}{\gamma} \\ \nabla \cdot \overline{H'm'_T} = P_T + Ex_{BT} + Ex_{AT} + \frac{(\gamma - 1)P_{ta}}{\gamma} \end{cases} \quad (21)$$

On the right-hand side of Eq. (21), terms in the form Ex_{ab} are energy exchange terms from a component and b component to the acoustic component (“A,” “B,” and “T” represent the acoustic, vortical, and thermal component, respectively). The thermal-acoustic source P_{ta} is split into two parts $\frac{P_{ta}}{\gamma}$ and $\frac{(\gamma - 1)P_{ta}}{\gamma}$, which affect the acoustic energy flux $\overline{H'm'_A}$ and the thermal energy flux $\overline{H'm'_T}$, respectively. Specifically,

acoustic source P_A is correlated with $\frac{P_{ta}}{\gamma}$ in the acoustic energy budget equation in Eq. (21). As shown in Figs. 8 and 9, $\frac{\sigma_{ta}}{\gamma}$ is perfectly balanced with σ_A except for the second mode. However, the difference between σ_A and $-\frac{\sigma_{ta}}{\gamma}$ for the second mode is small compared to the magnitude of σ_{ta} . Therefore, the net effect of σ_A and σ_{ta} can be approximated as $\frac{(\gamma - 1)\sigma_{ta}}{\gamma}$. Because the net effect of correlated σ_B and σ_T always stabilizes the mode S, it is concluded that the rise of the second mode is attributed to the thermal part of the thermal-acoustic source, $\frac{(\gamma - 1)P_{ta}}{\gamma}$.

VI. THERMAL-ACOUSTIC SOURCE

By analyzing the contribution of MPT sources to the growth rate σ of the mode S, the thermal part of the thermal-acoustic source $\frac{(\gamma - 1)P_{ta}}{\gamma}$ is revealed to be the cause of the modal growth of the second mode. In this section, the thermal-acoustic source P_{ta} is further analyzed based on the linearized energy conservation equation. Particularly, the viscous and inviscid effects are discussed in detail.

The linearization of the energy conservation equation for a 2D parallel flow field with unique mean pressure gives the following:

$$\rho T \left(\frac{\partial S'}{\partial t} + u \frac{\partial S'}{\partial x} + v' \frac{\partial S'}{\partial y} \right) = \Phi'. \quad (22)$$

Here, $\Phi = \nabla \cdot (k \nabla T) + \tau \cdot (\nabla \mathbf{u})$ includes both the thermal conduction effect and viscous dissipation effect. k is the coefficient of thermal conductivity. Equation (22) can be rewritten as follows:

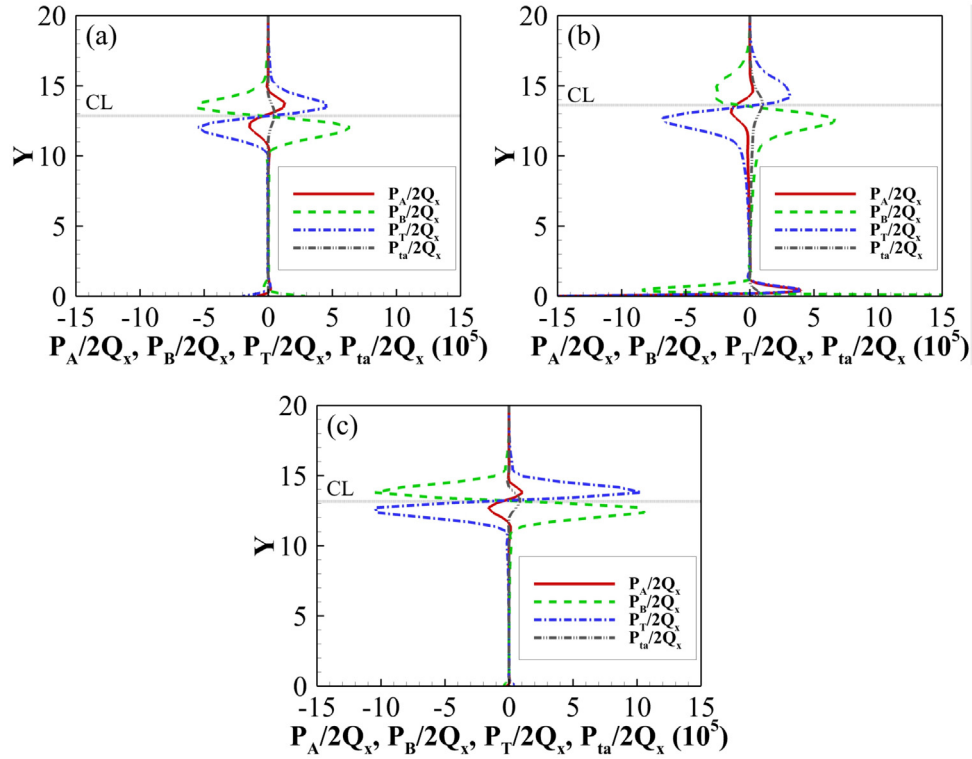


FIG. 5. Distribution of MPT sources of the mode S normalized by $2Q_x$ at $Re = 5000$ and $T_w = 1.0 T_r$ with (a) $\omega = 0.1$; (b) $\omega = 0.15$; and (c) $\omega = 0.2$. The location of the critical layer (CL) is marked with a horizontal dotted line.

$$\frac{\partial S'}{\partial t} + u \frac{\partial S'}{\partial x} = -v' \frac{\partial S}{\partial y} + \frac{\Phi'}{\rho T}. \quad (23)$$

The left-hand side of Eq. (23) is the rate of change in the fluctuation entropy observed in the reference frame with the mean streamwise velocity u . The first term on the right-hand side of Eq. (23), $-v' \frac{\partial S}{\partial y}$, is the entropy exchange between neighboring layers with different mean entropy due to normal fluctuation velocity, while the second term $\frac{\Phi'}{\rho T}$ is related to irreversible processes.

Considering disturbances with the harmonic waveform, we have the following:

$$\hat{S} = -\frac{\hat{v}}{i(xu - \omega)} \frac{\partial S}{\partial y} + \frac{1}{\rho T} \frac{\hat{\Phi}}{i(xu - \omega)}. \quad (24)$$

Equation (24) is valid for nonneutral instability waves. For a neutral instability wave, $(xu - \omega) = 0$ and $\frac{\Phi'}{\rho T} = v' \frac{\partial S}{\partial y}$ at the critical layer. However, we are concerned about the physical mechanism of the unstable second mode. The neutral instability wave case is not taken into consideration in the present study.

Furthermore, two new variables η and Ψ' are introduced as follows:

$$\frac{\partial \eta}{\partial t} + u \frac{\partial \eta}{\partial x} = v', \quad \frac{\partial \Psi'}{\partial t} + u \frac{\partial \Psi'}{\partial x} = \Phi'. \quad (25)$$

η is the disturbance displacement and Ψ' is the energy loss per volume due to the viscous effect observed in the reference frame with the mean streamwise velocity u .

The harmonic waveform of η and Ψ' is as follows:

$$\hat{\eta} = \frac{\hat{v}}{i(xu - \omega)}, \quad \hat{\Psi}' = \frac{\hat{\Phi}}{i(xu - \omega)}. \quad (26)$$

Then, Eq. (24) can be expressed as follows:

$$\hat{S} = -\hat{\eta} \frac{\partial S}{\partial y} + \frac{\hat{\Psi}'}{\rho T}. \quad (27)$$

Finally, we have

$$S' = -\eta \frac{\partial S}{\partial y} + \frac{\Psi'}{\rho T}. \quad (28)$$

The first part is fluctuation entropy caused by disturbance displacement between neighboring layers with different mean entropy. The second part is fluctuation entropy due to the dissipative effect (viscosity and thermal conductivity). Thus, the fluctuation entropy S' is considered to be composed of the “non-dissipative part” $S'_{nd} = -\eta \frac{\partial S}{\partial y}$ and the “dissipative part” $S'_d = \frac{\Psi'}{\rho T}$.

Furthermore, the thermal-acoustic source P_{ta} is split into two parts:

$$P_{ta} = \frac{p' \partial S'}{R \partial t} = -\frac{p' \partial \eta}{R \partial t} \frac{\partial S}{\partial y} + \frac{p' \partial \Psi'}{R \partial t}. \quad (29)$$

Again, the first part $-\frac{p' \partial \eta}{R \partial t} \frac{\partial S}{\partial y}$ is due to the non-dissipative effect denoted as P_{nd} and the second part $\frac{p' \partial \Psi'}{R \partial t}$ is due to the dissipative effect denoted as P_d .

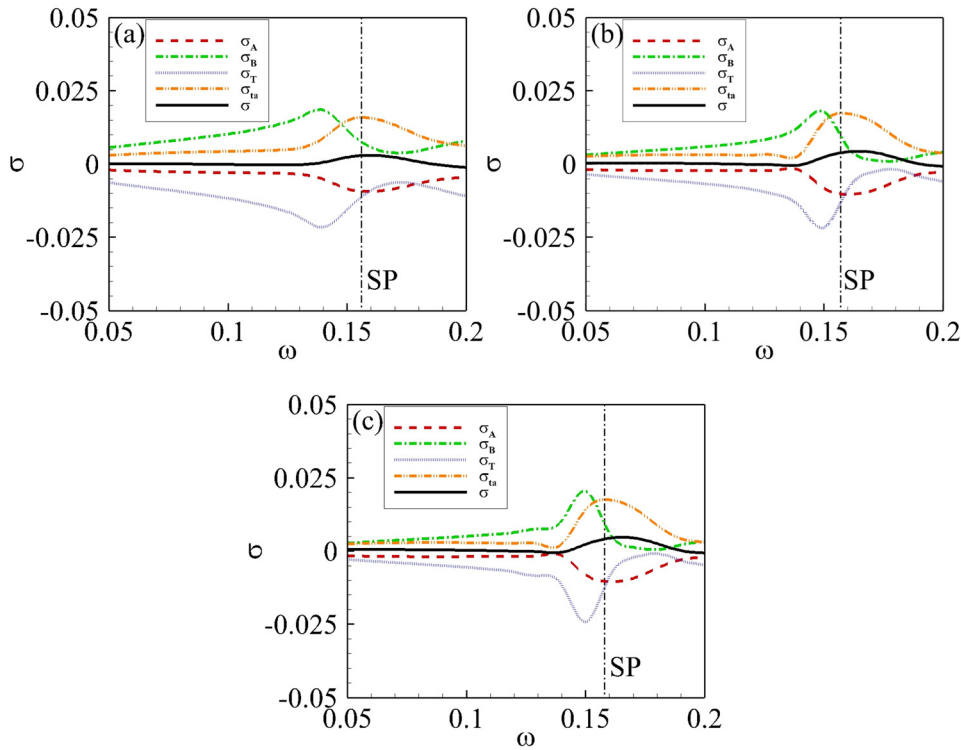


FIG. 6. Contribution of MPT sources on the growth rate σ of the mode S over the adiabatic wall with (a) $Re = 1000$, (b) $Re = 5000$, and (c) $Re = 9000$. The location of the synchronization point (SP) is marked with a vertical dashed-dotted line.

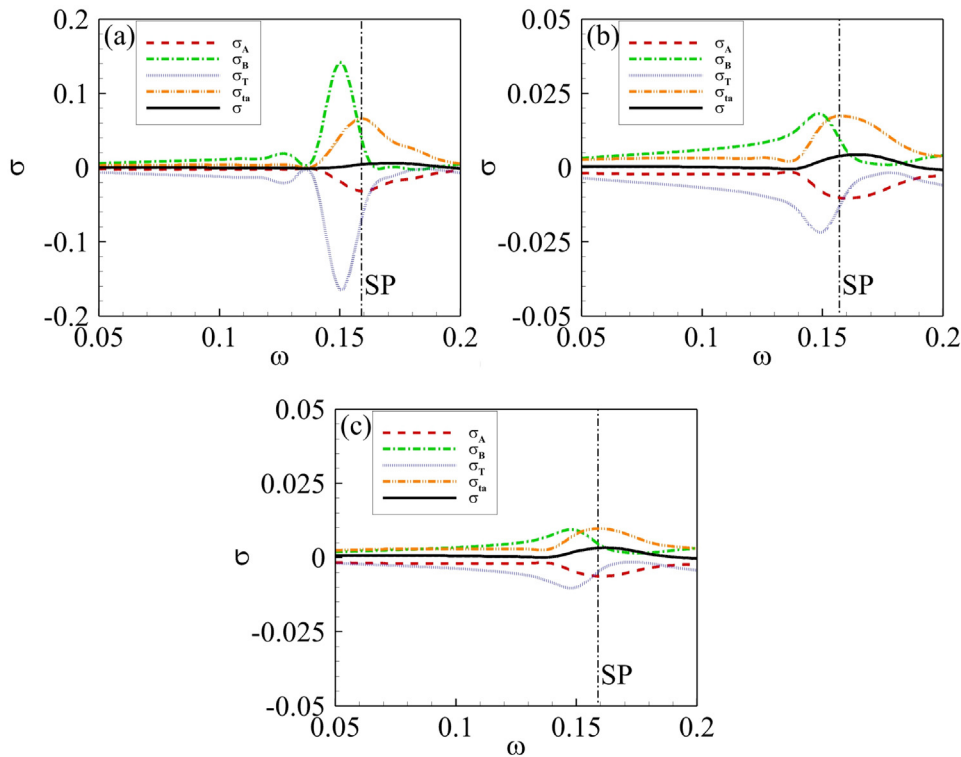


FIG. 7. Contribution of MPT sources on the growth rate σ of the mode S at $Re = 5000$ with (a) $T_w = 0.7 T_r$, (b) $T_w = 1.0 T_r$, and (c) $T_w = 1.3 T_r$. The location of the synchronization point (SP) is marked with a vertical dashed-dotted line.

27 August 2024 06:12:57

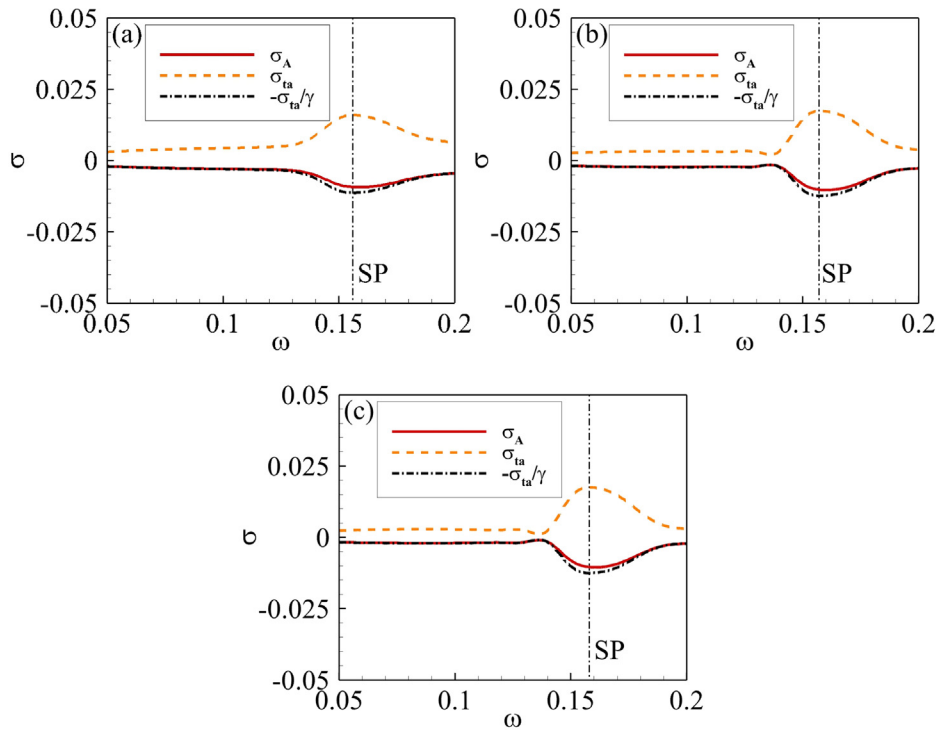


FIG. 8. Balance between σ_A and $\frac{\sigma_{ta}}{\gamma}$ over the adiabatic wall with (a) $Re = 1000$, (b) $Re = 5000$, and (c) $Re = 9000$.

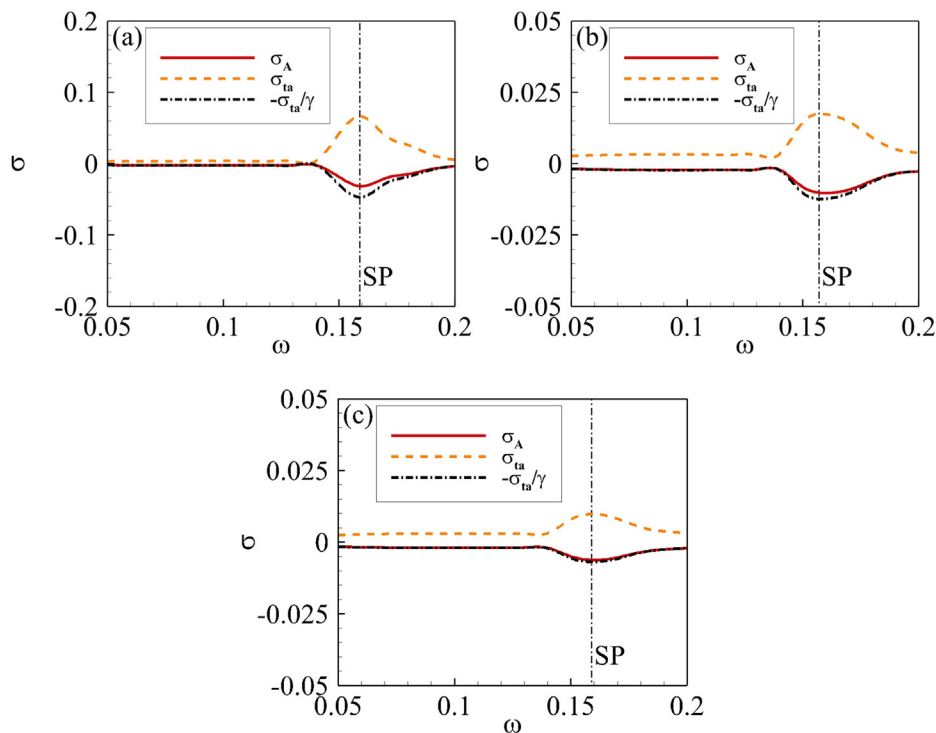


FIG. 9. Balance between σ_A and $\frac{\sigma_{ta}}{\gamma}$ at $Re = 5000$ with (a) $T_w = 0.7 T_r$, (b) $T_w = 1.0 T_r$, and (c) $T_w = 1.3 T_r$.

27 August 2024 06:12:57

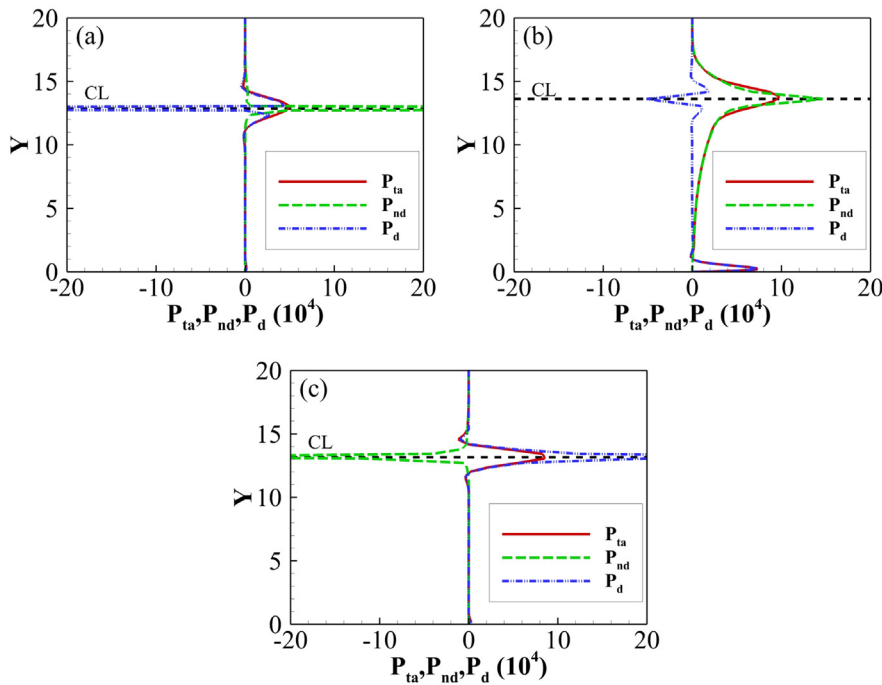


FIG. 10. P_{ta} , P_{nd} , and P_d normalized by $2Q_x$ at (a) $\omega = 0.1$; (b) $\omega = 0.15$; (c) $\omega = 0.2$ with $Re = 5000$, $T_w = 1.0 T_r$. The location of the critical layer (CL) is marked with a horizontal dashed line.

Figure 10 shows the P_{ta} , P_{nd} , and P_d (normalized by $2Q_x$) of the mode S at $\omega = 0.1, 0.15$, and 0.2 with $Re = 5000$, $T_w = 1.0 T_r$. Figure 11 shows the P_{ta} , P_{nd} , and P_d (normalized by $2Q_x$) of the mode S at $\omega = 0.15$ with different T_w and Re . In all cases, P_{ta} has

two positive peaks near the wall and the critical layer, which indicates that the thermal-acoustic source destabilizes the mode S effectively in these two regions. At the critical layer where singularity occurs in the inviscid case, both the magnitude of P_{nd} and

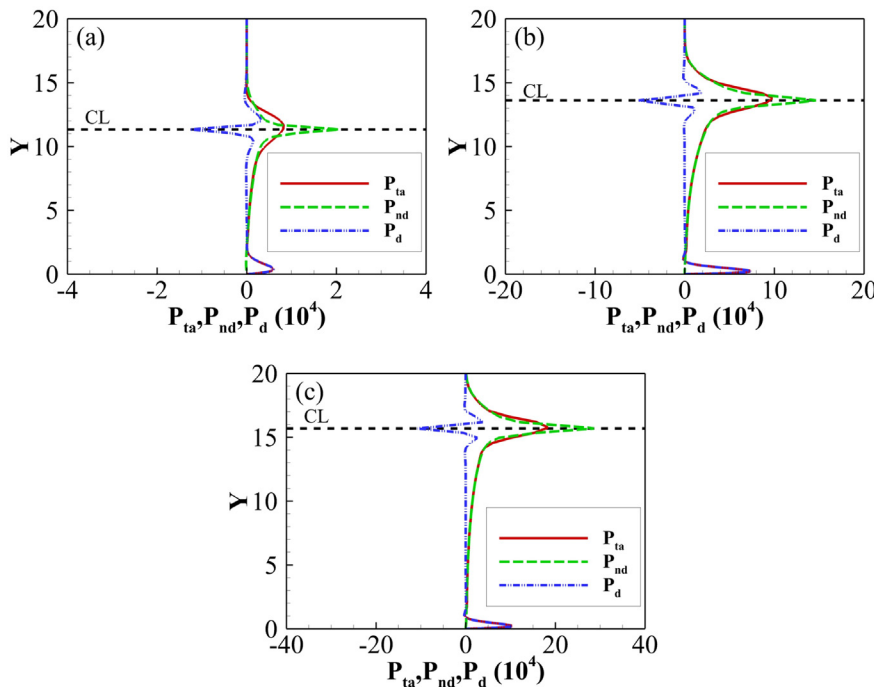


FIG. 11. P_{ta} , P_{nd} , and P_d normalized by $2Q_x$ at $\omega = 0.15$ with (a) $Re = 1000$, $T_w = 0.7 T_r$; (b) $Re = 5000$, $T_w = 1.0 T_r$; (c) $Re = 9000$, $T_w = 1.3 T_r$. The location of the critical layer (CL) is marked with a horizontal dashed line.

P_d become particularly large. At $\omega = 0.15$ (the second mode), P_{ta} always overlaps P_d near the wall. The viscous effect dominates the thermal-acoustic source near the wall for the second mode, while P_{nd} is negligible there. P_{nd} dominates the positive P_{ta} around the critical layer, especially for high Re cases. The results indicate that P_{nd} dominates and destabilizes the second mode around the critical layer, which is consistent with the inviscid nature of the second mode. At $\omega = 0.1$ and 0.2 , P_{ta} becomes negligible near the wall. P_d dominates P_{ta} in the vicinity of the critical layer except for a very small region where the inviscid singularity effect is significant. The results demonstrate that 1) the viscous and inviscid effects dominate the thermal-acoustic term P_{ta} for the second mode near the wall and the critical layer, respectively, and 2) the viscous effects dominate the thermal-acoustic term P_{ta} near the critical layer (except for a small region around the critical layer where the singularity effect arises) for mode S not related to the second mode.

VII. CONCLUSIONS

Theoretical analyses based on momentum potential theory were conducted to clarify the dominant source resulting in the amplification of the second mode in the Mach 6.0 boundary layer flow field. By integrating Doak's energy budget equation along the normal direction, the contribution of the MPT source term to the growth rate of the unstable mode S is identified. The vortical part σ_B is negatively correlated with the entropic part σ_T due to the vortical-entropy coupling effect, while the thermal-acoustic part σ_{ta} is negatively correlated with the acoustic part σ_A . The net effect of σ_B and σ_T is always negative, which stabilize the second mode. The net effect of σ_{ta} and σ_A can be approximated as the thermal part of σ_{ta} , $\frac{(\gamma-1)}{\gamma}\sigma_{ta}$, which is the cause of the amplification of the second mode. The pronounced positive peak of the thermal-acoustic source P_{ta} , appearing in the vicinity of the synchronization point, provides direct evidence that P_{ta} is the most likely to be responsible for the evolvment of the second-mode instability. The thermal-acoustic source P_{ta} is further split into the non-dissipative part and the dissipative part. The dissipative (viscous) thermal-acoustic source term destabilizes the second mode near the wall. In the vicinity of the critical layer, both dissipative (viscous) and non-dissipative (inviscid) terms can be responsible for the resulting positive thermal-acoustic contribution, depending on the wall temperature and Reynolds number. Although these results offer a new perspective to understand the modal growth of the second mode, the dynamic of instability needs further investigations.

ACKNOWLEDGMENTS

This work was supported by the National Natural Science Foundation of China, under Grant Nos. 12272049 and 11872116, and by the Research Grants Council of Hong Kong, under Contract No. 15216621/21E.

AUTHOR DECLARATIONS

Conflict of Interest

The authors have no conflicts to disclose.

Author Contributions

Tiehan Long: Conceptualization (lead); Formal analysis (lead); Software (equal); Writing – original draft (equal). **Peixu Guo:** Formal analysis (equal); Software (equal); Writing – original draft (equal). **Rui Zhao:** Funding acquisition (equal); Supervision (equal); Writing – review & editing (equal). **Chih-Yung Wen:** Funding acquisition (equal); Supervision (equal); Writing – review & editing (equal). **Feng Ji:** Supervision (equal); Writing – review & editing (equal).

DATA AVAILABILITY

The data that support the findings of this study are available from the corresponding author upon reasonable request.

APPENDIX A: STREAMWISE DERIVATIVE OF THE TIME AVERAGE TERM

In the 2D spatial LST, any two fluctuation quantities (real value) can be expressed as follows:

$$\begin{cases} f' = \hat{f} e^{-\alpha_i x + i(\alpha_r x - \omega t)} + \hat{f}^+ e^{-\alpha_i x - i(\alpha_r x - \omega t)} \\ g' = \hat{g} e^{-\alpha_i x + i(\alpha_r x - \omega t)} + \hat{g}^+ e^{-\alpha_i x - i(\alpha_r x - \omega t)} \end{cases}, \quad (A1)$$

where \hat{f} and \hat{g} are the complex-valued eigenfunctions of y in the wall normal direction, the superscript $+$ indicates the corresponding conjugate. The product of these two fluctuation quantities is as follows:

$$f'g' = \hat{f}\hat{g}e^{-2\alpha_i x + i2(\alpha_r x - \omega t)} + \hat{f}\hat{g}^+ e^{-2\alpha_i x} + \hat{f}^+\hat{g}e^{-2\alpha_i x} + \hat{f}^+\hat{g}^+ e^{-2\alpha_i x - i2(\alpha_r x - \omega t)}, \quad (A2)$$

due to

$$\int_0^{2\pi} \hat{f}\hat{g}e^{-2\alpha_i x + i2(\alpha_r x - \omega t)} dt = 0, \quad \int_0^{2\pi} \hat{f}^+\hat{g}^+ e^{-2\alpha_i x - i2(\alpha_r x - \omega t)} dt = 0. \quad (A3)$$

The time average of Eq. (A3) is as follows:

$$\overline{f'g'} = \frac{\omega}{2\pi} \int_0^{2\pi} f'g' dt = (\hat{f}\hat{g}^+ + \hat{f}^+\hat{g})e^{-2\alpha_i x}. \quad (A4)$$

Take partial differential of Eq. (A4) with x yields the following equation:

$$\frac{\partial \overline{f'g'}}{\partial x} = -2\alpha_i (\hat{f}\hat{g}^+ + \hat{f}^+\hat{g})e^{-2\alpha_i x} = -2\alpha_i \overline{f'g'}. \quad (A5)$$

Thus, we have

$$\frac{\partial (\overline{\rho u})'H'}{\partial x} = -2\alpha_i \overline{(\rho u)'H'} = 2\sigma \overline{(\rho u)'H'}. \quad (A6)$$

APPENDIX B: VERIFICATION

Figure 12 shows the comparison between both sides of Eq. (15) for the S mode with $Re = 5000$, $T_w = 1.0 T_r$. The difference between $\sigma = -\alpha_i$ and the sum of σ_B , σ_A , σ_T , and σ_{ta} is negligible.

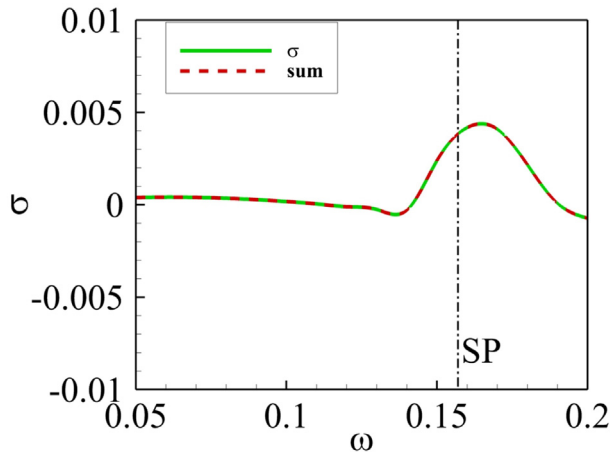


FIG. 12. Comparison of the growth rate $\sigma = -\alpha_i$ and the sum of σ_B , σ_A , σ_T , and σ_b .

REFERENCES

- ¹A. V. Fedorov, "Transition and stability of high-speed boundary layers," *Annu. Rev. Fluid Mech.* **43**, 79–95 (2011).
- ²M. Morkovin, E. Reshotko, and T. Herbert, "Transition in open flow systems: A reassessment," *Bull. Am. Phys. Soc.* **39**(9), 1882 (1994).
- ³J. M. Kendall, "Wind tunnel experiments relating to supersonic and hypersonic boundary-layer transition," *AIAA J.* **13**(3), 290–299 (1975).
- ⁴K. F. Stetson, E. R. Thompson, J. C. Donaldson, and L. G. Siler, "Laminar boundary layer stability experiments on a cone at Mach 8—Part I: Sharp cone," AIAA Paper No. 83-1761, 1983.
- ⁵S. J. Laurence, A. Wagner, and K. Hannemann, "Experimental study of second-mode instability growth and breakdown in a hypersonic boundary layer using high-speed schlieren visualization," *J. Fluid Mech.* **797**, 471–503 (2016).
- ⁶Y. Zhu, X. Chen, J. Wu, S. Chen, C. Lee, and M. Gad-el-Hak, "Aerodynamic heating in transitional hypersonic boundary layers: Role of second-mode instability," *Phys. Fluids* **30**(1), 011701 (2018).
- ⁷W. Zhu, M. Shi, Y. Zhu, and C. Lee, "Experimental study of hypersonic boundary layer transition on a permeable wall of a flared cone," *Phys. Fluids* **32**(1), 104110 (2020).
- ⁸L. M. Mack, "Boundary-layer stability theory," JPL Report No. 900-277 (Jet Propulsion Lab., Pasadena, CA, 1969).
- ⁹M. R. Malik, "Numerical methods for hypersonic boundary layer stability," *J. Comput. Phys.* **86**(2), 376–413 (1990).
- ¹⁰A. V. Fedorov and A. P. Khokhlov, "Prehistory of instability in a hypersonic boundary layer," *Theor. Comput. Fluid Dyn.* **14**, 359–375 (2001).
- ¹¹A. Tumin, "Three-dimensional spatial normal modes in compressible boundary layers," *J. Fluid Mech.* **586**, 295–322 (2007).
- ¹²X. Chen, Y. Zhu, and C. Lee, "Interactions between second mode and low-frequency waves in a hypersonic boundary layer," *J. Fluid Mech.* **820**, 693–735 (2017).
- ¹³Y. Ma and X. Zhong, "Receptivity of a supersonic boundary layer over a flat plate—Part 1: Wave structures and interactions," *J. Fluid Mech.* **488**, 31–78 (2003).
- ¹⁴Y. Ma and X. Zhong, "Receptivity of a supersonic boundary layer over a flat plate—Part 2: Receptivity to free-stream sound," *J. Fluid Mech.* **488**, 79–121 (2003).
- ¹⁵Y. Ma and X. Zhong, "Receptivity of a supersonic boundary layer over a flat plate—Part 3: Effects of different types of free-stream disturbances," *J. Fluid Mech.* **532**, 63–109 (2005).
- ¹⁶X. Zhong and X. Wang, "Direct numerical simulation on the receptivity, instability, and transition of hypersonic boundary layers," *Annu. Rev. Fluid Mech.* **44**(1), 527–561 (2012).
- ¹⁷A. Tumin, X. Wang, and X. Zhong, "Direct numerical simulation and the theory of receptivity in a hypersonic boundary layer," *Phys. Fluids* **19**, 014101 (2007).
- ¹⁸O. Reynolds, "On the dynamical theory of incompressible viscous fluids and the determination of the criterion," *Philos. Trans. R. Soc. A* **186**, 123–164 (1895).
- ¹⁹J. J. Kuehl, "Thermoacoustic interpretation of second-mode instability," *AIAA J.* **56**(9), 3585–3592 (2018).
- ²⁰X. Tian and C. Wen, "Growth mechanisms of second-mode instability in hypersonic boundary layers," *J. Fluid Mech.* **908**, R4 (2021).
- ²¹J. Rayleigh and R. B. Lindsay, *The Theory of Sound* (Dover Publications, 1945).
- ²²L. Kovásznay, "Turbulence in supersonic flow," *J. Aeronaut. Sci.* **20**(10), 657–682 (1953).
- ²³S. Unnikrishnan and D. V. Gaitonde, "Interactions between vortical, acoustic and thermal components during hypersonic transition," *J. Fluid Mech.* **868**, 611–647 (2019).
- ²⁴P. E. Doak, "Momentum potential theory of energy flux carried by momentum fluctuations," *J. Sound Vib.* **131**(1), 67–90 (1989).
- ²⁵T. Long, Y. Dong, R. Zhao, and C. Wen, "Mechanism of stabilization of porous coatings on unstable supersonic mode in hypersonic boundary layers," *Phys. Fluids* **33**(5), 054105 (2021).
- ²⁶G. Daviller, P. Comte, and P. Jordan, "Flow decomposition for the study of source mechanisms," AIAA Paper No. 2009-3305, 2009.
- ²⁷A. V. Fedorov and A. Tumin, "High-speed boundary-layer instability: Old terminology and a new framework," *AIAA J.* **49**(8), 1647–1657 (2011).